Fuel 113 (2013) 863–872

Contents lists available at SciVerse ScienceDirect

Fuel

journal homepage: www.elsevier.com/locate/fuel

Modelling of deposit formation and sintering for the co-combustion of coal with biomass

M.U. Garba, D.B. Ingham, L. Ma *, M.U. Degereji, M. Pourkashanian, A. Williams

CFD Centre, Energy Technology and Innovation Initiative, Faculty of Engineering, University of Leeds, Leeds LS2 9JT, UK

HIGHLIGHTS

- A computational fluid dynamics (CFD) model has been developed for the ash deposition rate.
- The CFD-based deposition model has been tested on two coals with three dissimilar biomasses.
- A numerical coal slagging index (NSI) has been employed to estimate the extent to which the deposits were sintered.
- Reasonably good agreement has been obtained for the CFD model and NSI.

ARTICLE INFO

Article history:
Received 29 September 2012
Received in revised form 15 December 2012
Accepted 18 December 2012
Available online 11 January 2013

Keywords:
Co-firing
CFD model
Ash deposition
Slagging index

ABSTRACT

During the combustion of coal and biomass blends, ash particles are deposited on the furnace wall, or on the heat transfer surfaces, and gradually they become sintered and harder. This makes it difficult to remove the deposits by soot blowing, and therefore manual cleaning is often required. In this paper, a computational fluid dynamics (CFD) model that predicts the deposition rates in boilers has been developed. This deposition model is based on the combined sticking probabilities of the ash particle viscosity and the melting behaviour of the ash particles. A numerical slagging index (NSI) is also employed to estimate the degree of the sintering of the deposits. The NSI is based on the ash viscosity, ash fusibility, ash chemistry and ash loading and the experimental data from the entrained flow reactor (EFR) at Imperial College, London, have been used to validate the models. We have found that the predicted results from the ash deposition model on the coal fired with short rotation crop (SRC) and miscanthus are reasonably consistent with the experimental measurements. Further, the NSI has been used to rank the investigated coal-biomass mixtures according to their degree of sintering.

1. Introduction

The co-firing of coal with biomass is an attractive option for power generation due to the substantial reductions of carbon dioxide (CO_2), nitric oxide (NO_x) and sulfur dioxide (SO_x) emissions [1]. Coal may be replaced partially, or almost entirely, by biomass in power generating plants, the extent depending on the economic and national energy policies that prevail at the time. Biomass co-firing takes advantage of the high efficiencies obtainable in coal-fired power plants and can be used with a wide range of coals and biomass.

Biomass can be divided into two main categories: woody fuels and agricultural residues (straw, olive waste). In a pulverized coal-fired power station, some ash particles impact on the heat transfer surfaces and are retained, forming deposits that cause slagging in the boiler or fouling in the convective pass. The use of biomass in coal fired plants may present additional technical problems. A major one is related to the low melting point of the biomass ash, which may create serious deposition problems. These deposits are removed naturally by shedding, or mechanically by soot blowing from a boiler, but because of the strength of certain deposits, boilers may be temporarily shut-down for manual cleaning. Both the strength of the deposit and the rate of the deposition are important. Further, the rate of ash deposition at operating conditions close to those for the real boilers are very difficult to be determined effectively. The major pathways for the ash particle transport to the boiler walls, inertial impaction, thermophoresis, heterogeneous reactions and condensation, have been well documented [2–4]. Nevertheless, the understanding of their pathways and thermal behaviour in terms of the quantitative deposit formation and the strength and degree of fusion on the heat transfer surface are still incomplete.

A number of experimental techniques have been adopted to study deposition under controlled conditions involving simplified laboratory rigs such as flow reactors [2,3,5–9]. However, many

* Corresponding author. Tel.: +44 (0) 1133438954.
E-mail address: l.ma@leeds.ac.uk (L. Ma).

0016-2361/$ - see front matter © 2013 Elsevier Ltd. All rights reserved.
http://dx.doi.org/10.1016/j.fuel.2012.12.065

Nomenclature

C	specific heat	U	velocity in the x-direction
C_d	spherical drag coefficient	V	velocity in the y-direction
Cs	thermal slip coefficient	α	particle static contact angle
C_t	numerical constant	γ	overall thermal based ash loading
D_p	diameter	γ_b	thermal based biomass ash loading
F	force	γ_c	thermal based coal ash loading
g	gravitational acceleration	δ	particle surface energy
h	convective heat transfer coefficient	ε_p	the particle emissivity
I	inertial deposition rate	η	impact efficient
m	mass	η_{m_i}	melt phase sticking probability
R	molar gas constant	η_{p_i}	viscosity sticking probability
Re	Reynolds number	θ_R	the radiation temperature
S	surface area	κ	fluxing oxide to sintering oxide
S_x	numerical slagging index	λ	gaseous mean free path
t	time	μ_f	critical viscosity
T	temperature	μ_p	particle viscosity
T_i	thermophoretic deposition rate	ρ_p	particle density
T_b	biomass ash softening temperature	σ	Stefan–Boltzmann constant
T_c	coal ash softening temperature	∞	bulk phase
T_s	overall softening temperature		

studies have been undertaken with large industrial boilers or large pilot combustion test facilities and the present situation with these are summarised in two recent Refs. [10] and [11] which also indicate the limitations in the CFD models. The entrained flow reactor (EFR) is often used because the temperature and reaction times can be accurately controlled [5–10]. Hutchings et al. [5] describe the design and operation of an EFR to assess the slagging propensity of a coal ash. Manton et al. [6] discussed coal ash slags and deposits from both single and blended fuels in an EFR. Borroso et al. [7] examined the slagging behaviour of coal blends under different operating conditions in an EFR. Wu et al. [8] have studied the co-combustion of coal with biomass up to 20 wt% of the total thermal input, and the influence of additives on the co-combustion was investigated. Wigley et al. [9] have presented experimental data on the deposition efficiency, as well as the extent to which the deposits were sintered for up to 60 wt% of coal replacement by biomass in an EFR. These investigations provide an objective assessment of the slagging propensity of coal ash and biomass and they can be run at varying deposition rates as needed. However, the major shortcoming of the EFR is the lack of a standard testing procedure.

There are no tools available that can unequivocally predict the slagging and fouling properties of any given fuel. The ash fusion temperature, ash viscosity, and ash chemistry are the three most basic tools employed for characterizing coal ash slagging and deposits during combustion [12]. Most of the ash deposits are derived from the minerals and inorganic components of coal, biomass and their blends. Their consolidation occurs by two main mechanisms: (i) viscous necking (flow sintering) of adjacent particles at a rate determined by the viscosity, and (ii) the bonding of particles by melting type or quantity [13,14]. The sintering between particles enhances the stickiness and increases the resistance to the thermal shock and erosion. In addition to the stickiness, the tendency of a particle to deposit is also affected by the particle surface energy and its static angle of impact. The effects of these factors have been tested in both biomass and coal combustion [10,11,15,16].

The ash fusion test (AFT) and cone deformation are other widely used tools that are employed in predicting the progress of the sintering mechanism [17]. The AFT, which determines the temperature at which the various stages of the ash softening and flow takes place, is based on the judgment of the analyst as to when the ash reaches and passes through the defined stages of the softening. Since the assessment of this method is subjective rather than objective, the results obtained may be misleading. Therefore the most frequently used parameter for correlating fusibility with its composition is the basic/acid (B/A) ratio. This is because an increase in the percentage of the basic component of the ash lowers the melting-point of the ash – the basic components are also known as the fluxing agents [18]. The ratio B/A, which was originally introduced for the assessment of coal ash, is restrictive and cannot be applied to certain types of biomass materials, especially those with a high phosphorus content in their ash. Although phosphorus is acidic, many publications, such as Kupka et al. [19], have shown that the presence of phosphorus acts as an additional fluxing agent for the development of the low-melting-point phases in the fly ash. Therefore, in order to account for this influence, the phosphorus contents have been added to the basic oxides [18,19].

Several attempts have been made to find reliable models to predict accurately the ash deposition rates in boilers. In particular, some models have used the particle viscosity as a function of temperature to determine the capture efficiency of the ash particles on impaction with the boiler walls for coal ash [2,15,20]. In the case of co-firing, the appearance of the melt phase is thought to increase not only the tendency for the ash particles to adhere to the furnace walls but also the rate at which the strength of the deposits build-up [21]. Computational fluid dynamic (CFD) models have been widely used [2,11,16,22,23] but at present some of these models suffer from a lack of accuracy since they rely on the modelling assumptions that have not been validated to a satisfactory level. However, CFD models often can predict the trends correctly, although in the case of coal-biomass co-combustion, additional complexities are introduced because of the behaviour of the ash [24–27].

Most papers that model ash deposition from co-combustion calculate the ash particle viscosity under high temperature regions to determine the particle collection efficiency [15,27]. Further, knowledge of the melting fraction and particle melting temperature in the high temperature region are also essential in determining the sticking probability. The effects of these criteria have been tested in biomass combustion but in the co-combustion of coal and biomass little has been reported. Most of the experimental studies

on biomass co-firing have suggested that the viscosity and melting fraction are the key requirements for determining the ash stickiness [9,19,27]. However, so far no modelling investigations have taken advantage of combining the effects of these components in determining the particle collection efficiency.

The object of this paper is to develop a CFD-based model to predict the deposit formation and the extent to which the deposits are sintered. The paper draws upon the experimental results from Imperial College EFR for the rates of the deposition and sintering of the coal and biomass blends [9]. A comparison is made between these results and the computed data and the validity of the deposition model discussed. The numerical slagging index (NSI), previously proposed [15], is tested with the results from these coal/biomass mixtures.

2. Theoretical model

2.1. Combustion models

In the modelling of the deposition rates, accurate calculations of the temperature field is a key issue since it influences the mass, size and composition of the particles that may impact on the deposition surface. In the devolatilization step, the volatile matter (gases and tars) from the thermal decomposition of the coal leaves the particles. A number of devolatilization network codes have been developed in the literature for coal, biomass and their blends [24]. We have used combustion sub-models that have been previously used and validated by the authors [24,25]. The model uses a two-step reaction mechanism for the volatile combustion and the eddy dissipation model was used to couple the turbulence and the chemical reactions. Further, the char combustion sub-model is based on the Smith intrinsic model [28].

2.2. Particle trajectories

In addition to solving the transport equations for the gaseous phase (Eulerian frame of reference), a discrete second phase (spherical particles) is simulated in a Lagrangian frame of reference. In this framework, the transport of the solid fuel particles is governed by the particle momentum equation, written in its one-dimensional form for the x-direction in a Cartesian coordinate system, as follows [2]:

$$\frac{dU_p}{dt} = F_D + F_g + F_v + F_t \tag{1}$$

where U_p is the velocity of the particle, F_D, F_g, F_v and F_t are the x-components of the drag, gravitational, virtual mass and thermophoretic forces, respectively, that are acted on a unit mass of the particle, and the trajectory of particle in the x-direction is resolved by the equation [2]:

$$\frac{dx}{dt} = U_p \tag{2}$$

The drag force on each particle may be estimated by using the following equation [2,29]:

$$F_D = \frac{18\mu C_d \mathrm{Re}}{\rho_p D_p^2 24}(U - U_p) \tag{3}$$

where μ is the viscosity of the gas, ρ_p and D_p are the density and diameter of the particle, respectively, U is the gas velocity, C_d is the drag coefficient that frequently is obtained experimentally, and it may be expressed as a function of the particle Reynolds number Re [30].

The Reynolds number is determined as follows [2]:

$$\mathrm{Re} = \frac{\rho D_p |U - U_p|}{\mu} \tag{4}$$

where ρ is the density of the gas.

The virtual mass force is given by [29]:

$$F_v = \frac{\rho}{2\rho_p}\frac{d}{dt}(U - U_p) \tag{5}$$

The thermophoretic force due to the local temperature gradient in the gas flow in the x-direction is calculated as follows [29]:

$$F_t = -\frac{6\pi D_p \mu^2 c_s (K + c_t Kn)}{\rho(1 + 3c_m Kn)(1 + 2K + 2c_t Kn)}\frac{1}{m_p T}\frac{\partial T}{\partial x} \tag{6}$$

where the Knudsen number $Kn = 2\lambda/D_p$ [29],

$$\lambda = \left(\sqrt{\frac{\pi}{2}}\frac{\mu}{p}\sqrt{RT}\right) \tag{7}$$

and $K = k_\infty/k_p$, $c_m = 1.14$, $c_s = 1.17$, $c_t = 2.18$, R is the gas constant and T is the temperature of the gas.

The energy balance equation of a fly-ash particle, which is solved along its trajectory, in order to obtain the corresponding temperature at the point of impact, is given as follows [29]:

$$m_p C_p \frac{dT_p}{dt} = hA_p(T_\infty - T_p) + \varepsilon_p A_p \sigma(\theta_R^4 - T_p^4) \tag{8}$$

where m_p is the mass of the particle, C_p is the specific heat of the particle, T_p is the particle temperature, h is the convective heat transfer coefficient and T_∞ is the bulk phase temperature. The second term on the right hand side of the Eq. (8) is the heat transfer due to the radiation, ε_p is the particle emissivity, σ is the Stefan–Boltzmann constant, and θ_R is the radiation temperature relating to the radiation intensity.

2.3. Deposition models

The major ash deposition mechanisms during coal and biomass combustion are the inertial impaction ($I.\eta$), thermophoresis (T), condensation (C) and chemical reaction (R) [4]. A deposition rate based on these mechanism is described by

$$\frac{dm}{dt} = I.\eta + T + C + R \tag{9}$$

During the first stage in the formation of the deposits, the alkali salts condense on the heating surface. In this case, the metal surface controls the deposition. However, in the case where the temperature on the heat transfer surface is set at higher temperatures ($\geqslant$1250 °C), the slagging mechanism becomes more of a bulk property of the mixed fuel than a surface issue. Therefore Eq. (9) reduces to the following:

$$\frac{dm}{dt} = I.\eta \tag{10}$$

The stickiness of the coal ash is determined from the viscosity-based models, while the stickiness of the biomass ash is determined from its melt fraction and the particle softening temperatures. Since a particle and deposit layer consists of a mixture of salt and silica rich material, the sticking probabilities of both the coal ash viscosity and the melting components of the biomass have been combined as follows:

$$\eta = x\eta_c + y\eta_b \tag{11}$$

where x, y, η_c and η_b are the ratios of the coal in the blend, the ratio of the biomass in the blend, the coal ash sticking probability and the biomass ash sticking probability, respectively.

For the coal ash sticking model, the sticking probability is primarily concerned with the viscosity of the fly ash. Further, the fly

ash viscosity is linked to the configuration of the oxide melt, and it is very sensitive to the changes in the temperature and composition. In this case, the sticking probability is defined as the ratio of the critical viscosity, μ_f, and the particle viscosity, μ_p, at a certain temperature [2]. The assumption is that any impact that involves any viscosity below a critical value results in the particle sticking to the heat transfer surface. Therefore, the particle stickiness can be expressed as follows:

$$\eta_{c_i} = \frac{\mu_f}{\mu_p}, \quad \text{where } \mu_p > \mu_f \text{ and } \eta_{p_i} = 1, \quad \text{where } \mu_p \leqslant \mu_f \tag{12}$$

A number of different values have been suggested for the critical viscosity, as discussed by Huang et al. [2], and this paper a value of 10^5 Pa s was adopted following the suggestion of Degereji et al. [15]. The particle viscosity (Pa s), as a function of the particle temperature, can be calculated from the Watt–Fereday model [31] as follows:

$$\mu_p = 10^{y-1} \tag{13}$$

where

$$y = 10^7 m/(T-150)^2 + c \tag{14}$$

$$m = 0.00835\ (SiO_2) + 0.00601\ (Al_2O_3) - 0.109$$

$$c = 0.0415\ (SiO_2) + 0.0192\ (Al_2O_3) + 0.0276\ (Fe_2O_3) + 0.016\ (CaO) - 3.92$$

and the values for the two parameters, namely the slope, m, and the intercept, c, are computed from the species concentration in weight percentages of the ash with the following assumption [32]:

$$(SiO_2) + (Al_2O_3) + (Equiv.\ Fe_2O_3) + (CaO) + MgO = 100\ wt\% \tag{15}$$

For biomass ash, a combination of the particle softening temperature and the melting fraction has been used to estimate the stickiness of the particle and both are related to the salt material within the biomass particle. According to Ma et al. [16], a particle would be perfectly sticky when it has been completely melted and the softening temperature of the biomass can be estimated using the following empirical equation:

$$T_b = 1.81(CaO) + 4.20(Al_2O_3) - 2.41(K_2O) + 5.31(P_2O_5) + 1017\ ^\circ C \tag{16}$$

where CaO, Al_2O_3, K_2O and P_2O_5 are the relative mass concentrations of these species in the biomass ash and they are normalized so that they sum to 100%.

However, when a particle has not burnt out completely, only a fraction of the melt will be sticky. In other words if the temperature of the particle has reached the melting temperature of the potassium species (about 700 °C), or other salts, but has not yet reached the particle softening temperature estimated by Eq. (16), the potassium or salt species will be melted and the following expression is used to calculate the sticking probability of the biomass ash:

$$\eta_{b_i} = \frac{m_{silicate}}{m_{salt}+m_{silicate}} . f_{melt,silicate} + \frac{m_{salt}}{m_{salt}+m_{silicate}} . f_{melt,salt} \tag{17}$$

where m_{salt}, $m_{silicate}$, $f_{melt,salt}$ and $f_{melt,silicate}$ are the mass of the salt, the mass of the silica, the melt fraction of the salt and the melt fraction of the silica, respectively. While $m_{silicate}$ and m_{salt} are estimated from the equilibrium calculation, $f_{melt,silicate}$ and $f_{melt,salt}$ are obtained from the melting curves of the potassium and silica particles, respectively [33].

In the modelling work of Kaer [33], it has been assumed that the mass of the molten phase is non-sticky if the mass of the molten phase is below 15%. Between 15% and 70%, the mass of the molten phase is assumed to be sticky. Above this percentage, the mass of the molten phase is assumed to be flowing. Further, the thermodynamic equilibrium calculations are used to calculate the amount of the melt fraction considering the possible phases of the liquid slag and solid solution.

Establishing whether a colliding particle actually sticks or rebounds from the heat transfer tube begins with the calculation of the excess energy. This is in addition to the stickiness of the particle on the deposit surface. In order to represent this numerically, a rebound criterion, as derived by Mueller et al. [14] is employed. The rebound tendency has previously been assumed to be a function of the viscosity, impact velocity and static angle of the particle [34]. If a particle possesses the necessary excess energy, E_x (>0), the particle is judged to bounce off the surface, otherwise it will stick. The particle excess energy is calculated using the following empirical formula [14,32]:

$$E_x = \frac{D^2}{4}(1-\cos\alpha) - \frac{3D^{2.3}}{25}(1-co\alpha)^{0.63} + \frac{2}{3D} - 1 \tag{18}$$

where D is the ratio of the maximum deformation of the particle diameter to the actual particle diameter and this ratio is related to the particle Weber number and the Reynolds number as follows:

$$D = (12+We)^{1/2}[3(1-\cos\alpha) + 4(We/\mathrm{Re}^{1/2})]^{1/2} \tag{19}$$

The Weber number is defined as follows:

$$We = \frac{\rho_p U_p^2 D_p}{\delta} \tag{20}$$

where α is the static contact angle and δ is the particle surface tension.

A numerical slagging index (NSI) previously developed has been implemented for various coals and their blends [35] was modified to account for the coal/biomass blend. The NSI is generally expressed in terms of the incoming ash, γ and the ash viscosity, μ, as follows [35]:

$$S_X = \gamma/\mathrm{Log}(\mu) \tag{21}$$

For coal/biomass blends, the effects of the biomass addition can be predicted on the deposit sintering by determining the viscosity of the blend ash from the ash content and the ash chemistry of the individual fuels [9]. Thus, the weight of the incoming ash has been defined in terms of the content of the ash and the heating value of the individual fuels as follows:

$$\gamma = x\gamma_c + y\gamma_b \tag{22}$$

where γ_c and γ_b are the weight of the coal ash and the weight of the biomass ash, respectively. Also, the modified Watt-Fereday ash viscosity model used previously [31] has been redefined as in equation (13) in order to account for the softening temperatures of both the coal (T_c) and the biomass (T_b) as defined in Eqs. (25) and (16), respectively, as follows:

$$\mathrm{Log}(\mu) = \frac{m.10^7}{T_s^2} + c \tag{23}$$

$$T_s^2 = xT_c^2 + (y/\kappa)T_b^2) \tag{24}$$

$$T_c = a(SiO_2) + b(Al_2O_3) + c(Fe_2O_3) + d(CaO) + e(MgO) + f(\alpha) + g + 150\ ^\circ C \tag{25}$$

where the factor, κ (fluxing-sintering oxides) [18,19] in Eq. (24), is introduced and it is estimated as follows:

$$\kappa = \frac{Fe_2O_3 + CaO + MgO + Na_2O + K_2O + (P_2O_5)}{SiO_2 + Al_2O_3 + TiO_2} \quad (26)$$

3. Model implementation

3.1. Source of experimental data

The furnace used for this study was the Imperial College EFR as represented in Fig. 1. The measurement techniques employed and the data obtained were reported by Manton et al. [6] and Wigley et al. [9] and these are summarized as follows. The reactor consists of an assembly of four electrically heated furnaces, approximately 5 m long vertical tube and with a diameter 100 mm. These furnaces comprise of three heating elements; molybdenum disilicide ($MoSi_2$), silicon carbide (SiC) and two Kanthal AF wire (FeCrAl alloy) that heat the reactor body, thus providing a temperature gradient from 1650 °C at the top to 1200 °C at the bottom. A series of joints between each furnace facilitates the introduction of probes, which allows the ash and char samples to be withdrawn from the combustion. The gas temperatures at the ports 1 and 2 are approximately 1400 °C and 1250 °C, respectively. Further, uncooled ceramic probes have been used to collect the ash deposits and the burner section consists of the primary inlet through which the primary air and the pulverized coal are fed, and the secondary air inlet for the hot swirling air. The coal flow rate of 0.014 gs^{-1} was used, the primary air flow rate was 0.067 kgs^{-1} at 70 °C, and the secondary air flow was 1.167 kgs^{-1} at 300 °C.

The effects of the five types of biomass have been studied: miscanthus, short rotation coppice (SRC), olive residue, palm kernel expeller cake and sawmill residue. The two coals used, Russian and South African, are typical bituminous UK power station coals with high and low slagging potentials, respectively.

Coal was blended for each of the five biomasses 0, 20, 40 and 60 wt% of the fuel. The fuel samples studied were dried, milled and sieved so that their diameters were less than 100 μm. The samples were then blended for 15 min, and all feeds were dried at 120 °C in nitrogen gas prior to use. 100 g of fuel mixture was run for a duration of 30 min, and the deposit sample was collected on probe 2 which is located in the midsection of the EFR. The probe has thermocouples that register the surface temperature of the deposits. Our understanding of the paper is that the experiments were run as sets of data for each biomass since the experimental conditions changed slightly from set to set as described in Section 4.3.

Naturally, fouling occurs on the convective heat surfaces, while the slagging is formed on the furnace wall, or on the partially fouled wall (convective surfaces exposed to radiant heat). In many studies using an EFR [5–7,9], a mullite probe is used for the deposit collection rather than a metallic probe since it (i) provides a porous ceramic surface, which is very similar to a partially fouled wall in comparison to the polished surface of the metallic probe, and (ii) the long exposure time that occurs during the formation of the initial deposit layer on the metallic surfaces is avoided.

3.2. CFD model

In the present study, the computational simulations of the EFR has been performed using the commercial CFD code, FLUENT version 13.0.0 [29]. To reduce the computational complexity, symmetrical conditions were assumed. This resulted in a model of one half of the EFR and then the use of the symmetry to predict the full domain solution. In the work by Hutchings et al. [5], the deposits were collected at the probe position, where the gas temperature is about 1400 °C on an uncooled ceramic probe are generally of highly fused nature and give little indication of the likely slagging propensity of the coal. However, when deposits are collected at the probe position, where the gas temperature is about 1250 °C on an uncooled ceramic probe, they range from a thin dusty covering of lightly sintered ash particles to well-bonded and coherent deposits. The type of the deposit depends on the nature and proportions of the mineral matter present in the fuel. Further, the deposits collected under these conditions closely resemble those sintered deposits from the bulk ash on the furnace walls and the superheaters of large furnaces and therefore are suitable for characterization. For this reason, the samples of fly ash particles inside the EFR considered in the experimental work of Wigley et al. [9] were collect on mullite tube 2 set at a temperature 1250 °C. As a consequence, mullite probe 1 (port 1) was not considered in the CFD build-up of the present calculations. The grid used to model the combustion using the EFR contains approximately 1,200,000 cells and the burner region is shown in Fig. 2. The particle sizes were distributed between 1 and 95 μm in 10 injection groups, with a mean particle

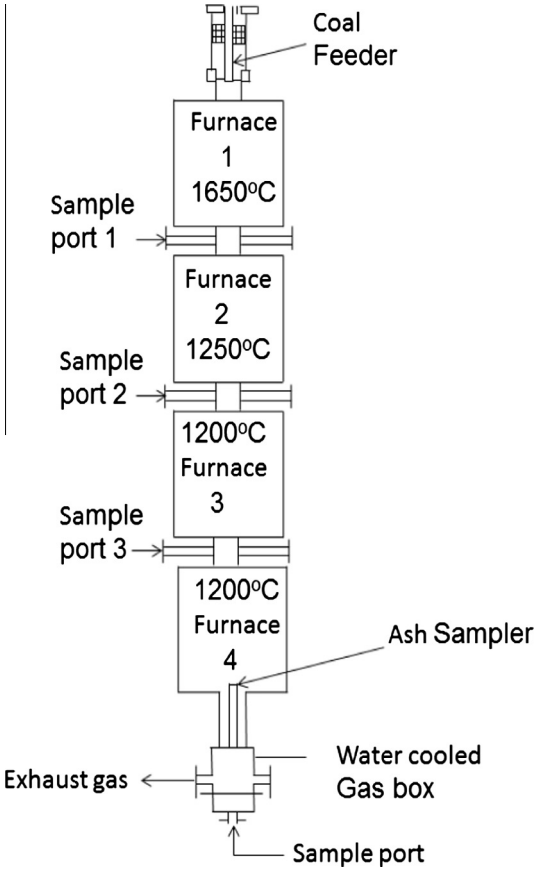

Fig. 1. Schematic diagram of the Imperial College EFR based on [5,6].

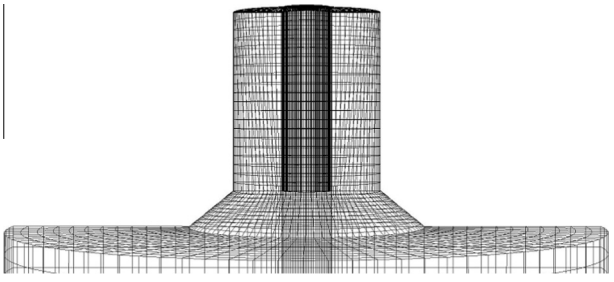

Fig. 2. Geometry details of EFR in the near burner region.

size of 85 μm and a spread parameter 1.3 has been used. The mesh was refined to yield about 1.2 million cells, and it was found that the gas temperature and the velocity profiles show no significant difference between using 1.0 and 1.2 million cells. Therefore, the prediction results have been obtained using 1.2 million computational cells. The deposition code, Eqs. (11)–(18), has been developed and was compiled and linked to the main code in FLUENT. The main code in FLUENT calculates the particle trajectories while the role of the deposition code is to add stickiness to the particle as it is being transported from the combustion zone to the furnace wall or the heat transfer surface.

3.3. Fuel properties

The properties of the coal and biomass are given in Table 1. With differing chemical properties in the ash content between the five biomasses investigated, their slagging tendencies vary with the level of the biomass addition [9]. The deposition model is limited to only SRC, miscanthus and olive that are fairly rich in alkali content. Palm was not modelled because of the lack of appropriate information on the melting behaviour of the phosphorus ash. However, all the five biomass materials were employed in the NSI calculation. The data from miscanthus, olive, palm, SRC and sawmill were taken from the 'Phyllis' biomass database [36], while the ash content and its composition were taken from Wigley et al. [9].

4. CFD predictions and discussions

4.1. Gas phase and particle temperatures

The furnace temperature is of importance since it is closely related to the deposition potential on the heat transfer surface. Fig. 3a and b shows the predicted particle and gas temperatures for pure coal. The combustion of the injected particles starts immediately after the particles have mixed with the oxidizing air at the exit of the burner. This is promoted by the recirculation zone observed in the vicinity of the burner. Further, the particles are rapidly heated by radiation from the hot reactor walls.

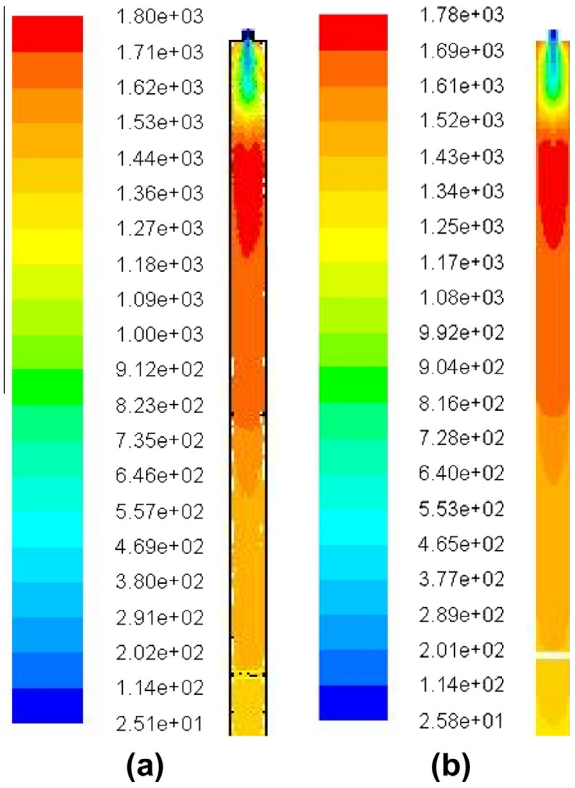

Fig. 3. Contours of the furnace temperature (°C) in a vertical plane of the furnace studied (a) particle (b) gas.

It can be observed that the majority of the particles within the vicinity of the burner reach a temperature of about 1500–1600 °C, where large numbers of the particles melt. These particles are completely fused and potentially flow around the mullite probe or the furnace wall when they impact on a surface or wall. For this reason, as previously explained, the deposition probe 1 was not considered in this calculation. In a particle temperature range of about

Table 1
Coal and biomass ash content (wt%) and chemical composition (wt%) [9,32].

Component	Russian coal	Miscanthus	Olive	Palm	Short rotation crop	Sawmill
Proximate analysis	wt% On dry basis					
Volatiles	30	83.5	79.0	77.1	80.5	81.2
Fixed carbon	76	29.3	33.1	34.0	32.1	31.6
Moisture	5.56	30.7	24.0	23.0	18.5	19.0
Ash	12.6	2.3	5.7	4.2	2.4	2.5
CV(MJ/kg)	27	18.5	22.0	21.4	18.7	19.1
Ultimate analysis	wt% On dry basis					
C	76.5	48.1	42.2	4.31	50.2	50.1
H	4.5	5.8	5.1	5.1	5.9	6.2
O	4.9	41.9	45.6	45.2	42.2	42.4
N	1.9	0.3	1.62	1.51	0.1	0.5
S	0.4	0.1	N/A	N/A	N/A	0.05
Cl	0.25	0.16	N/A	N/A	N/A	0.013
Ash composition	wt% On dry basis					
SiO_2	60.1	57.0	32.1	15.1	17.3	40.7
Al_2O_3	24.0	2.4	6.6	3.2	4.4	8.1
Fe_2O_3	6.0	3.4	4.9	5.3	3.8	3.8
CaO	4.1	10.0	12.4	10.7	33.3	28.6
MgO	1.1	3.1	12.2	12.0	8.6	4.1
K_2O	3.0	18.2	18.9	9.7	13.8	6.8
Na_2O	0.4	1.1	0.4	0.3	1.0	1.1
TiO_2	1.2	0.2	0.2	0.1	0.3	1.1
MnO	0.1	0.4	0.0	1.0	0.4	3.6
P_2O_5	0.0	4.2	12.2	42.7	17.0	2.1

N/A = not available.

1250–1400 °C, which corresponds to the position where probe 2 is located, the particles have been reported to display a semi-molten, more compact aspect and potentially remain sticky on the mullites upon impaction [5,6]. However, particles that emerge from the burner and those in the lower section of the EFR experience lower particle temperatures. A temperature range of about 1250–1800 °C has been obtained in the vertical plane of the furnace which is in reasonably good agreement with the measured data which is in the temperature range 1200–1700 °C. The values are slightly over predicted by only about 6% and therefore this gives confidence in the accuracy of the coal combustion model.

The predicted gas temperature profiles in the boiler for pure coal firing and blends with SRC for up to 60% co-firing ratio are presented in Fig. 4. For the co-firing ratio of 20 wt%, the temperature profile does not differ significantly from that for pure coal. However, for a co-firing ratio greater than 20 wt%, a significant difference is observed. The results show that the temperature of the gas at the exit of the furnace decreases when the proportion of the SRC blended with coal increases.

4.2. Gas velocity

Fig. 5a illustrates the gas velocity on the symmetry plane of the EFR. It can be observed from the figure that the mixing of the air and the fuel near the burner exit is promoted by means of the recirculating flow produced by the motion of the primary air and the strong swirling motion of the secondary air. Since, in the EFR, the particles are entrained into the gas flow, the flow of the gas down the centre of a 0.1 m diameter tube (see Fig. 5a) indicates the absence of any dispersion which causes the particles to experience differing flow velocities and residence times.

Many publications (for example [5,6,8]) have shown that the combusting gas flow produced by the EFR under well-controlled conditions is necessary for the precise determination of the particle heating rates and this is considered as an advantage over the use of large rigs. The velocities introduced at the two air inlets (see Fig. 5a), which evolves into a single peak velocity, has adequately captured this advantage. A peak velocity of about 4.2 ms^{-1} is obtained for the hot travelling gas at corresponding temperatures of about 1600 °C. The gas velocities in the central region of the EFR have been found to be approximately twice the average velocity and this is in good agreement with what has been reported by Hutchings et al. [5]. Further, we have found that the radial velocity profile decreases from the peak values on the centreline, to almost zero on either side of the reactor wall.

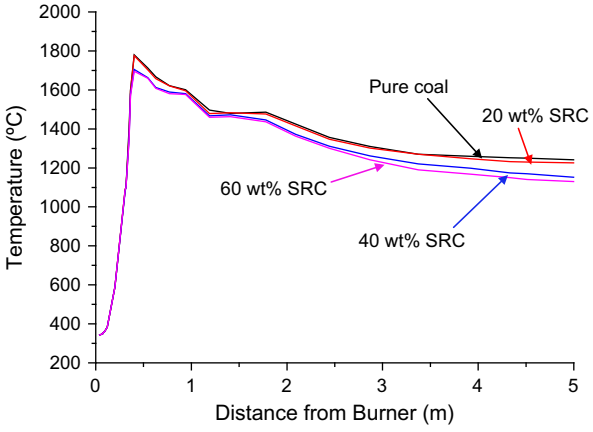

Fig. 4. Gas temperatures (°C) on the vertical axis for four thermal shares of the coal with SRC.

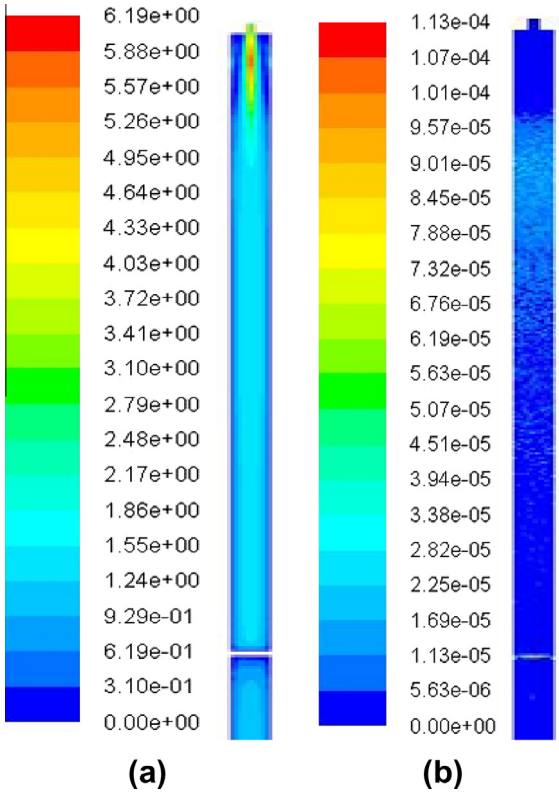

Fig. 5. Contour of the (a) gas velocity (m/s) on the symmetry plane and (b) particle deposition rates (kg/m^2 s) on the furnace wall and probe 2.

4.3. Deposition rates

A view of the EFR deposits on a deposition probe can be seen in Fig. 5b. The operating conditions used as the boundary conditions for both the coal and coal/biomass blends are the same. Fig. 5b shows that the deposition occurs on the furnace walls and on the mullite probe. Close to the burner, it can be seen that the reactor walls initially contains no deposits, and then the deposits are formed rapidly at about 0.2 m away from the burner exit by the impacting ash particles. The impacting ash particles that remain on the heat transfer surface have been reported to constitute most of the deposits formed on the pulverized furnace walls [5]. These ash particles may possess sufficient inertia to transverse the boundary layer and impact on the furnace walls. In addition, the intensity of the volatile combustion results in a zone of sharp temperature rise and a significant number of the particles soften, thereby increasing the tendency to stick to the walls. Due to the streamline flow of the particles under the influence of gravity, a high concentration of deposits (slagging intensity) has been found in the central region of the mullite probe. Another factor that contributes to the high concentration of the deposits in the central region of the mullite probe is due to the high degree of carbon burn out that occurs further downstream where the probe 2 was located. However, at a lower section of the EFR, the ash particles are less sticky due to the lower temperatures in this region.

A photograph of the ash deposition on the probe after 30 min of exposure time for pure coal [9] is shown in Fig. 6a. The dark part in the photograph shows the deposits scattered over the probe with most of them are concentrated in the central region of the probe and all on the upper surface. The predicted deposition pattern (see Fig. 6b) is reasonably consistent with that observed experimentally, particularly in the central region. This indicates that

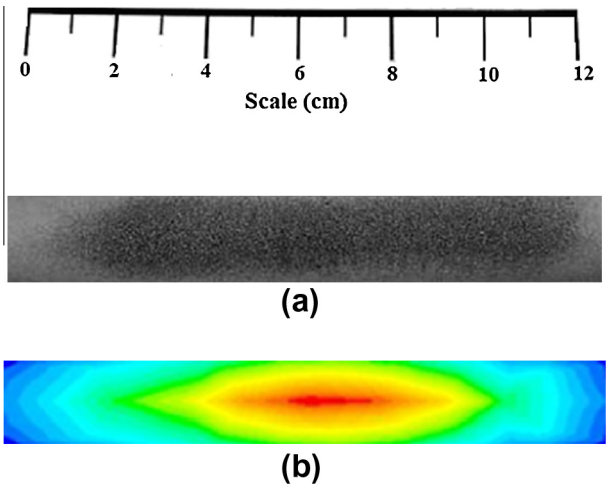

Fig. 6. Visual comparison between the experiment [9] and the computation.

the model is valid and has provided the right qualitative prediction which serves as a basis for quantitative validation.

The deposits collected on the mullite probes were first characterised by the deposition efficiency. Tables 2a and 2b shows the deposition efficiency (the proportion of incident ash retained on the probe) on a probe which has been calculated during the co-combustion of coal and different masses of the biomass materials in the EFR [9]. The deposition efficiency was calculated for each EFR run based on the mass percentage of the fuel ash calculated that impacts on the projected surface area of the probe that was retained in the collected deposit. The projected surface area is calculated from the probe outer diameter of 20 mm and the EFR inner tube diameter 100 mm. Two coals, Russian and South African, and three biomass, SRC, Miscanthus and Olive waste were studied. Although the experiment has been performed under identical operating conditions as that for pure coal, the variability in the deposition efficiency was observed in the experimental data. According to the authors, the source of the variability is associated with the heating condition to the operational temperature and the final setup. Five measurements were made for the Russian coal alone and the deposition efficiencies varied from 4.7 to 14.40 wt% collection efficiency, with an average of 9.5%. In order to compute the experimental results on an equal basis, all the experimental results were normalized so that the 0 wt% biomass addition was the mean value. These results are shown in Table 2a. In Table 2b the same biomass were studied using South African coal. The same issue in variability was observed but for this set of results the results were normalized to 9.1%. Further, palm waste was not computed because of the high level of phosphorus present in it.

Table 2a
Comparison between the computed and the measured data for Russian Coal and different levels of biomass.

Biomass	Level of biomass addition (wt%)			
	0	20	40	60
SRC experimental	14.4	11.6	19.7	13.3
SRC normalized to 9.5%	9.5	7.7	13.0	8.6
SRC computed	11.3	13.9	18.1	16.0
Miscanthus experimental	4.7	5.6	6.3	6.1
Miscanthus normalized to 9.5%	9.5	11.3	12.6	12.2
Miscanthus computed	11.3	7.6	8.1	8.5
Olive experimental	13	15.2	13.4	9.7
Olive normalized to 9.5%	9.5	11.1	9.8	7.1
Olive computed	11.3	15.2	14.1	14.9

Table 2b
Comparison between the computed and the measured data for South African Coal and different levels of biomass.

Biomass	Level of biomass addition (wt%)			
	0	20	40	60
SRC experimental	10.2	4.1	12.7	14.6
SRC normalized to 9.1%	9.1	3.7	11.3	13.0
SRC computed	10.1	10.1	10.3	10.8
Miscanthus experimental	8.0	8.2	10.3	12.7
Miscanthus normalized to 9.1%	9.1	9.3	11.7	14.5
Miscanthus computed	10.1	11.5	12.3	13.1
Olive experimental	10.9	11.8	11.5	16.4
Olive normalized to 9.1%	9.1	9.9	9.6	14.6
Olive computed	10.1	11.2	12.7	14.0

In the case of the Russian coal, the deposition efficiency of 20 wt% SRC is lower than that of the 100% coal combustion. A primary reason for this is that the coal ash is diluted by the low iron biomass ash during co-combustion, thereby decreasing the amount of iron introduced into the furnace. Another reason for the deposition efficiency reduction may be related to the relatively high calcium content in the ash of the SRC, which may generate calcium components with a high melting point. In the experimental results, it was observed for all the biomass studied that the deposition increases to about 60% and then decreases. This pattern is observed for the SRC computations but not for miscanthus or olive. Further, this trend is nonlinear and may be caused by many factors, including the significant reduction in the blend ash, the possibility of erosion effects on the deposits, etc.

A similar situation holds for the South African Coal. Other authors have observed similar nonlinear ash deposition behaviour in their experiments [21,27].

4.4. Sintering of the deposits: Performance of NSI

After characterising the deposit by calculating the deposition efficiency, the deposits were further characterised by the SEM and the extent to which the deposits were sintered was presented in [9]. The NSI was developed in such a way that all the indicators for the deposit strength and degree of fusion have been combined together. The viscosity is at the root of the deposition problems; consequently it was the first considered by the NSI, Eq. (21). Based on the performance of the NSI in Fig. 7 (each bar represents the

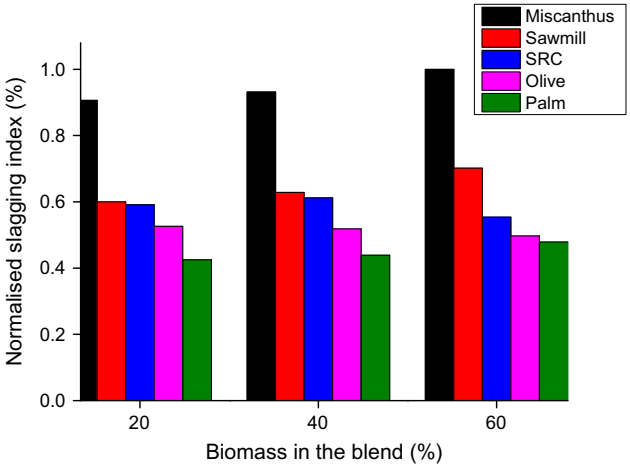

Fig. 7. The degree of the sintering for a mixture of coal with biomass.

Table 3
Numerical Slagging Index compared with experiment and slag viscosity index.

Sintering behaviour	Ranking of the sintered deposits
Experiment Wigley et al. [9]	Miscanthus < Sawmill < SRC < Olive < Palm
Slag viscosity index Wigley et al. [9]	Miscanthus < Sawmill < SRC < Palm = Olive
NSI (present work)	Miscanthus < Sawmill < SRC < Olive < Palm

coal-biomass mix) the miscanthus fuel mix has the highest normalized slagging index and this corresponds to the weakest deposit. The ash property of the miscanthus is comparable to the coal ash property. For example, the high content of the SiO_2 (>50%) in the solid fuel ash is an attribute well known for coal [37]. Further, the SiO_2 possess strong covalent bonds and large amounts of silica in the coal (>50%) and miscanthus (>50%) ash blend (see Table 1) may lead to a high melting point and hence a low deposition potential.

Another indicator for the rate of the deposit sintering, which the NSI has considered, is the melting characteristic of the viscous ash particles. Although the AFT analyses do not indicate exactly at what temperature the first melt/slag occurs, AFT and cone deformation experiments provide an estimate of the ash melting phase where the fluxing agents can be strongly sticky. While pure compounds of potassium have a melting point of 774 °C (KCl) and 1069 °C (K_2SO_4) [38], pure compounds of the phosphorus melt at 583 °C (P_2O_5) [16]. The high content of the phosphorus in palm kernel cake ash (P_2O_5 content >SiO_2 content in the ash) is given in Table 1 and this indicates the formation of the low melting phase which is responsible for the yielding of the strongest deposit. This can be observed in Fig. 7 with the coal-palm mix, showing the lowest bar in Fig. 7 in all the co-firing ratios. In addition to the AFT, the effect of the ash chemistry has also been captured by modifying the softening temperature in order to recognize the fluxing/bonding elements to an adequate degree. For dry ash and high melting temperatures, the value of κ in Eq. (26) is low. As the content of the fluxing agents increases in the fuel mixture, the ash becomes stickier and the ash melting temperatures begin to decrease. Table 3 shows a comparison between the experiment data and the predictions. It is observed that the degree of the deposit sintering observed in the EFR deposits increase in the order: Miscanthus < Sawmill < SRC < Olive < Palm. The results of the NSI show that the miscanthus is the least in terms of the slagging, followed by sawmill, then SRC, followed by olive and palm is the highest. This ranking of the NSI does agree with the observations of the EFR deposits, but it does not agree with the slag viscosity index as defined in [9]. This is because the model adopted in the calculated viscosity (Kalmanovitch and Frank method [39]) does not take into account the role of the phosphorus and the prediction may be misleading, especially at higher levels of biomass addition.

5. Conclusions

The deposition model, based on the combined sticking probabilities of the ash particle viscosity and the melting behaviour of the ash particle has been developed. This is suitable for the prediction of the deposition rates of heterogeneous coal/biomass ash slag in a high temperature region.

The deposition efficiencies in the EFR were computed for the coal with three different biomass materials using a CFD code and the results obtained are compared with the experimental data. Reasonably good agreement was obtained.

A NSI used previously by some of the authors has been modified to account for the differing chemical composition of the biomass ash and it has successfully ranked the deposits according to the degree of sintering. It has been observed that there are significant differences in the degree of sintering between blends ash of the parent fuels. The reasons for this are mainly due to the differences in the ash chemistry between the parent fuels.

Acknowledgments

The authors wish to thank Professor J. Williamson, Imperial College, London, for his very helpful advice. M.U. Garba would like to thank the Petroleum Technology Development Fund (PTDF) of the Federal Republic of Nigeria for funding his research studies.

References

[1] Williams A, Pourkashanian M, Jones JM. The combustion of coal and some other solid fuels. Symp (Int) Combust 2000;28(2):2141–62.
[2] Huang LY, Norman JS, Pourkashanian M, Williams A. Prediction of ash deposition on superheater tubes from pulverized coal combustion. Fuel 1996;7:271–9.
[3] Lee FCC, Lockwood FC. Modelling ash deposition in pulverized coal-fired applications. Prog Energy Combust Sci 1999;25:117–32.
[4] Baxter LL, DeSollar RW. A mechanistic description of ash deposition during pulverized coal combustion: predictions compared with observations. Fuel 1993;72:1411–8.
[5] Hutchings IS, West SS, Williamson J. An assessment of coal-ash slagging propensity using an entrained flow reactor. In: Baxter L, DeSollar R, editors. Proceeding of a conference on Applications of Advanced Technology to Ash-Related Problems in Boiler. Proceedings of the Engineering Foundation Conference. Waterville Valley, New Hampshire. Plenum Press New York; 1995 vol. 1621. p. 201–22.
[6] Manton NJ, Williamson J, Riley GS. Changes in slagging behaviour with composition for blended coals. In: Proceeding of an engineering foundation conference on Impact of mineral impurities in solid fuel combustion Kona. Kluwer Academic/Plenum Publication New York; 1997. p. 297–03.
[7] Barroso J, Ballester J, Ferrer LM, Jiménez S. Study of coal ash deposition in an entrained flow reactor: influence of coal type, blend composition and operating conditions. Fuel Process Technol 2006;87:737–52.
[8] Wu H, Glarborg P, Frandsen FJ, Dam-Johansen K, Jensen PA, Sander B. Co-combustion of pulverized coal and solid recovered fuel in an entrained flow reactor – general combustion and ash behaviour. Fuel 2011;90:1980–91.
[9] Wigley F, Williamson J, Malmgren A, Riley G. Ash deposition at higher levels of coal replacement by biomass. Fuel Process Technol 2007;88:1148–54.
[10] Ma Z, Iman F, Lu P, Sears R, Kong L, Rokanuzzaman AS, et al. A comprehensive slagging and fouling prediction tool for coal-fired boilers and its validation/application. Fuel Processing Technol 2007;88:1035–43.
[11] Weber R, Mancini M, Schaffel-Mancini N, Kupka T. On predicting the ash behaviour using Computational Fluid Dynamics CFD. Fuel Processing Technol 2013;105:113–28.
[12] McLennen AR, Bryant GW, Bailey CW, Stanmore BR, Wall TF. Index for iron-based slagging for pulverized coal firing in oxidizing and reducing conditions. Energy Fuel 2000;14:349–54.
[13] Backman R, Hupa M, Skrifvars B-J. Predicting superheater deposit formation in boilers burning biomass. In: Proceeding of the conference on impact of mineral impurities in solid fuel combustion; 1997. p. 405–16.
[14] Mueller Ch, Selenius M, Theis M, Skrifvars B-J, Backman R, Hupa M, et al. Deposition behaviour of molten alkali-rich fly ashes–development of submodel for CFD applications. Proc Combust Inst 2005;30:2991–8.
[15] Degereji MU, Ingham DB, Ma L, Pourkashanian M, Williams A. Prediction of ash slagging propensity in a pulverized coal combustion furnace. Fuel 2011;101:171–8.
[16] Ma L, Pourkashanian M, Williams A, Jones JM. A numerical model for predicting biomass particle deposition in a pf furnace. In: Proc ASME 2006, Barcelona, Spain. GT2006-90356; 2006. p. 333–42.
[17] Gupta SK, Wall TF, Creelman RA, Gupta RP. Ash fusion temperatures and the transformations of coal ash particles to slag. Fuel Process Technol 1998;56:33–43.
[18] Pronobis M. The influence of biomass co-combustion on boiler fouling and efficiency. Fuel 2006;85:474–80.
[19] Kupka T, Mancini M, Irmer M, Weber R. Investigation of ash deposit formation during co-firing of coal with sewage sludge, saw-dust and refuse derived fuel. Fuel 2008;87:2824–37.
[20] Rushdi A, Gupta R, Sharma A, Holcombe D. Mechanistic prediction of ash deposition in a pilot-scale test facility. Fuel 2005;84:1246–58.
[21] Heinzel T, Siegle V, Spliethoff H, Hein KRG. Investigation of slagging in pulverized fuel co-combustion of biomass and coal at pilot-scale test facility. Fuel Process Technol 1998;54:109–25.
[22] Vuthaluru R, Vuthaluru HB. Modelling of a wall fired furnace for different operating conditions using FLUENT. Fuel Process Technol 2006;87(7):633–9.

[23] Garba MU, Ingham DB, Ma L, Porter RTJ, Pourkashnian M, Tan HZ, et al. Prediction of potassium chloride sulfation and its effect on deposition in biomass-fired boilers. Energy Fuels 2012;26(11):6501–8.
[24] Ma L, Gharebaghi M, Porter R, Pourkashanian M, Jones JM, Williams A. Modelling methods for co-fired fuel furnaces. Fuel 2009;88:2448–54.
[25] Backreedy RI, Fletcher LM, Jones JM, Ma L, Pourkashanian M, Williams A. Cofiring pulverized coal and biomass: a modelling approach. Proc Combust Inst 2005;30:2955–64.
[26] Forstner M, Hofmeister GM, Joller J, Dahl M, Braun S, Kleditzsch R, et al. Oberberger. CFD simulation of ash deposit formation in fixed bed biomass furnaces and boilers. Prog Comput Fluid Dyn 2006;6(4/5):248–61.
[27] Zheng Y, Jensen PA, Jensen AD, Sander B, Junker H. Ash transformation during co-firing coal and straw. Fuel 2007;86:1008–20.
[28] Smith IW. The combustion rates of coal chars: a review. Symp (Int) Combust 1982;19(1):1045–65.
[29] Fluent Inc., Ansys Fluent User's Guide 2009. Release 12.0, Fluent Inc., Lebanon, NH; 2009.
[30] Morsi SA, Alexander AJ. An investigation of particle trajectories in two-phase flow systems. J Fluid Mech 1972;55(2):193–208.
[31] Watt JD, Fereday F. The flow properties of slags formed from the ashes of british coals: part 1 viscosity of homogeneous liquid clags in relation to slag composition. J Inst Fuel 1969;42:99–103.
[32] Vargas S, Frandsen FJ, Dam-Johansen K. Rheological properties of high – temperature melts of coal ashes and other silicates. Prog Energy Combust Sci 2001;27:237–429.
[33] Kaer, SK. Numerical investigation of deposit formation in straw-fired boilers, PhD diss., Aalborg University; 2001.
[34] Mao T, Kuhn DC, Tran H. Spread and rebound of liquid droplets upon impact on flat surfaces. AIChE J 1997;43(9):2169–79.
[35] Degereji MU, Ingham DB, Ma L, Pourkashanian M, Williams A. Numerical assessment of coals/blends slagging potential in pulverized coal boilers. Fuel 2012;102:345–53.
[36] Phyllis. Database, Energy Research Centre of the Netherlands; 2004. <http://www.ecn.nl/phyllis.
[37] Zhang L, Jahanshahi S. Modeling viscosity of alumina-containing silicate melts. Scand J Metall 2001;30:364–9.
[38] Cook LP, McMurdie HF. Phase diagrams for ceramists, volume VII, The America Ceramic Society, Westerville, OH, USA; 1989, Fig. 7106 (ISBN 0-944904-04-1).
[39] Kalmanovitch DP, Frank M. An effective model of viscosity for ash deposition phenomena. In: Engineering foundation conference on mineral matter and ash deposition from Coal. Santa Barbara, CA: United Engineering Trustees Inc.; 1988.